

The radio-bright accreting millisecond X-ray pulsar IGR J17591–2342

T. D. RUSSELL,¹ N. DEGENAAR,¹ R. WIJNANDS,¹ J. VAN DEN EIJNDEN,¹ N. V. GUSINSKAIA,^{1,2} J. W. T. HESSELS,^{1,2} AND
J. C. A. MILLER-JONES³

¹*Anton Pannekoek Institute for Astronomy, University of Amsterdam, Science Park 904, 1098 XH, Amsterdam, The Netherlands*

²*ASTRON, Netherlands Institute for Radio Astronomy, Oude Hoogeveensedijk 4, 7991 PD, Dwingeloo, The Netherlands*

³*International Centre for Radio Astronomy Research - Curtin University, GPO Box U1987, Perth, WA 6845, Australia*

(Received 2018; Revised 2018; Accepted ...)

Submitted to ApJL

ABSTRACT

IGR J17591–2342 is a 527-Hz accreting millisecond X-ray pulsar that was discovered in outburst in 2018 August. In this paper, we present quasi-simultaneous radio and X-ray monitoring of this source during the early part of the outburst. IGR J17591–2342 is highly absorbed in X-rays, with an equivalent hydrogen absorption along the line of sight, N_{H} , of $\approx 4.4 \times 10^{22} \text{ cm}^{-2}$, where the Galactic column density is expected to be $\approx 1.12\text{--}1.44 \times 10^{22} \text{ cm}^{-2}$. The high absorption suggests that the source is either relatively distant ($>5 \text{ kpc}$), or the X-ray emission is strongly absorbed by material local to the system. Radio emission detected by the Australia Telescope Compact Array shows that, for a given X-ray luminosity and for distances greater than 3 kpc, this source was exceptionally radio loud when compared to other accreting neutron stars in outburst ($L_{\text{X}} > 10^{33} \text{ erg s}^{-1}$). For most reasonable distances, IGR J17591–2342 appeared as radio luminous as actively accreting, stellar-mass black hole X-ray binaries.

Keywords: X-rays: binaries – stars: neutron – pulsars: general – radio continuum: stars – ISM: jets and outflows, abundances, dust, extinction – stars: individual (IGR J17591–2342)

1. INTRODUCTION

Accreting millisecond X-ray pulsars (AMXPs) are binary systems in which a neutron star (NS) primary accretes material — often only sporadically — from a low-mass companion star. However, in contrast to the majority of known neutron star X-ray binaries (NSXRBs), these objects show X-ray pulsations as material is channelled from the disk onto the magnetic poles of the rotating NS (e.g. [Wijnands & van der Klis 1998](#)). These objects are thought to be the link between accreting low-mass X-ray binaries (XRBs) and millisecond pulsars (MSPs; see [Wijnands & van der Klis 1998](#); [Patruno & Watts 2012](#), for review) where the transfer of angular momentum during the accreting XRB phase can spin up the NS to millisecond periods (e.g. [Alpar et al. 1982](#); [Radhakrishnan & Srinivasan 1982](#)). This link has

been exemplified, e.g., by the systems PSR J1023+0038 and M28I (IGR J18245-2452), which have been observed to transition between radio MSP and AMXP states on relatively short timescales ([Archibald et al. 2009](#); [Papitto et al. 2013](#); [Stappers et al. 2014](#)). Such transitional MSPs (tMSPs) are also thought to switch between accretion-powered and rotation-powered pulsar states.

AMXPs are typically transient, going through cycles of outburst and quiescence (e.g. in 't Zand et al. 1998). During outburst, radio emission with a flat or inverted spectrum ($\alpha \approx 0$, where the flux density, S_{ν} , scales with the frequency, ν , such that $S_{\nu} \propto \nu^{\alpha}$) is observed (e.g. [Tudor et al. 2017](#)), indicative of a partially self-absorbed, compact jet (e.g. [Blandford & Königl 1979](#)).

In their hard X-ray states at the beginning and end of a typical outburst, black hole (BH) XRBs exhibit a tight, non-linear relationship between their radio (L_{R}) and X-ray (L_{X}) luminosities that extends over several decades in luminosity (e.g. [Gallo et al. 2012](#); [Corbel et al. 2013](#)). The observed empirical relationship

is generally described by two distinct power-law tracks in the radio/X-ray luminosity plane; an upper ‘radio-loud’ track with a best fitting slope of $L_R \propto L_X^{0.6}$ and a lower, steeper, ‘radio-quiet’ track with a best fitting slope of $L_R \propto L_X^{-1}$ (Gallo et al. 2012). However, recently the statistical significance of the two separate tracks has been questioned (Gallo et al. 2014, 2018). Also, individual systems have shown significant deviation over luminosity ranges spanning <2 orders of magnitude (e.g. Corbel et al. 2013).

For accreting NSs the picture is even less clear. Not only is the connection complicated by the presence of a stellar surface/magnetosphere (e.g. Maccarone 2008), but also NSs appear fainter in the radio than their BH counterparts (e.g. Fender & Kuulkers 2001; Migliari & Fender 2006), meaning that their L_R/L_X behaviour has generally been measured across a smaller dynamic range (and with lower detection significance) than their BH counterparts. Initially, a steep ~ 1.4 correlation was suggested (Migliari & Fender 2006). However, individual systems appear to show varying correlation indices and normalisations, and not all follow similar, or even well-defined tracks (e.g. Tudor et al. 2017). To try to account for the restricted luminosity ranges that NS systems have typically been monitored over, regression analysis of a large sample of hard state NS systems showed that NSs as a whole appear to be a factor of ~ 22 fainter than the population of hard state BHs, but with a similar correlation slope (Gallo et al. 2018).

The differences in both normalisation and slope for individual systems could be driven by a number of factors, such as jet power, compact object mass, spin, magnetic field, and jet launching mechanism. Recent results showing faint radio jets being launched from a slowly-spinning high-magnetic field ($>10^{12}$ G) accreting NS indicate that the magnetic field or spin of the NS could be playing an important role in the radio brightness (van den Eijnden et al. 2018b).

1.1. IGR J17591–2342

IGR J17591–2342 was discovered in outburst by the INTERNATIONAL Gamma-Ray Astrophysics Laboratory (INTEGRAL) on 2018 August 10–11 (MJD 58340–58341), during monitoring of the Galactic center (Ducci et al. 2018). Its position was refined by the Neil Gehrels Swift Observatory (*Swift*) X-ray telescope (XRT) (Bozzo et al. 2018) and archival all-sky *Swift* Burst Alert Telescope (BAT) observations indicate that the outburst rose above detection threshold around 2018 July 22 (MJD 58321), ~ 20 days earlier (Krimm et al. 2018). We observed the source at radio wavelengths using the Australia Telescope Compact Array (ATCA),

detecting bright radio emission, leading to our initial suggestion that the source may be a BH candidate (Russell et al. 2018). However, coherent X-ray pulsations at 527.4 Hz (1.9 ms) detected using the Nuclear Spectroscopic Telescope Array (*NuSTAR*) and the Neutron star Interior Composition Explorer (*NICER*) identified this source as an AMXP (Ferrigno et al. 2018; Sanna et al. 2018), with an orbital period of ~ 8.8 hours and a companion mass of $\gtrsim 0.42 M_\odot$. Assuming a $1.4 M_\odot$ NS mass and typical AMXP parameters, the spin frequency derivative implies a magnetic field of $1.4 \times 10^8 < B < 8 \times 10^9$ G (Sanna et al. 2018). After discovery, the source stayed active for ~ 80 days, exhibiting some long term variability, including multiple re-brightenings (e.g. Sanchez-Fernandez et al. 2018).

In this paper, we discuss quasi-simultaneous radio and X-ray observations taken in the early stages of the outburst (spanning MJDs 58344–58356). The high X-ray absorption suggests that the source is relatively distant and therefore much more radio luminous than that from other known NS systems. We investigate the implications of this radio brightness in the context of other known XRBs.

2. OBSERVATIONS

2.1. ATCA radio observations

We conducted DDT radio observations (project ID: CX413) with the Australia Telescope Compact Array (ATCA). IGR J17591–2342 was observed three times early in its outburst, on 2018 August 14, 19, and 25 (MJDs 58344, 58349, and 58355, respectively; see Table 1). The observations were taken at central frequencies of 5.5 and 9 GHz. The August 25 observations had additional frequencies of 17 and 19 GHz recorded. Each frequency pair was taken simultaneously, and all bands were recorded with a bandwidth of 2 GHz. PKS 1934–638 was used for flux calibration, while phase calibration was carried out using 1817–254 on August 14 and with 1752–225 on August 19 and 25. The data were flagged and calibrated following standard procedures within the Common Astronomy Software Applications (CASA v4.7; McMullin et al. 2007).

For the August 14 observation the telescope was in a relatively extended (1.5D) configuration. Imaging was carried out with Briggs weighting (robust=0), to minimise effects from diffuse emission in the field due to its location towards the Galactic center, providing angular resolutions of $6.8'' \times 1.4''$ at 5.5 GHz and $3.9'' \times 0.9''$ at 9 GHz (with a position angle 15 degrees North of East). The flux density was determined by fitting for a point source in the image plane. From this epoch, we measure a (9 GHz) right ascension (R.A.) and declination (Dec.)

Table 1. ATCA radio observations of IGR J17591–2342. MJDs note the mid-point of the observation, with the quoted uncertainties reflecting the observation duration.

Date	MJD	Frequency (GHz)	Flux density (mJy)	α
2018 Aug 14	58344.56±0.12	5.5	1.09±0.02	0.1±0.3
		9.0	1.12±0.02	
2018 Aug 19	58349.26±0.07	5.5	1.00±0.05	−0.30±0.25
		9.0	0.85±0.05	
2018 Aug 25	58355.28±0.12	5.5	1.18±0.04	0.25±0.1
		9.0	1.21±0.04	
	58355.28±0.10	17.0	1.54±0.10	
		19.0	1.60±0.09	

of:

R.A. (J2000) = 17^h59^m02^s.86 +/- 0.04,
 Dec. (J2000) = -23°43^m08^s.3 +/- 0.1,

where the uncertainties are from the fitted position of the point source, which are larger than the theoretical statistical error from beam centroiding.

For our August 19 and 25 observations, ATCA was in a compact (H75) configuration, where five of the six antennas are located within 75 meters of each other. Due to significant diffuse emission, imaging was not trivial. However, ATCA’s sixth antenna is located 6 km from the array core. Using only the longest baselines out to antenna six to eliminate issues from diffuse emission, we determined the source flux by fitting the target (and other sources in the field) in the uv-plane using UVMULTIFIT (Martí-Vidal et al. 2014).

Source flux densities from UVMULTIFIT, or IMFIT in CASA are presented in Table 1.

2.2. *Swift* X-ray observations

Swift-XRT observed IGR J17591–2342 every few days during the outburst (target IDs: 10803 and 10804). Observations closest in time to our ATCA monitoring (within 1 day) were extracted with the *Swift*-XRT online pipeline (Evans et al. 2009), from which the spectral files and associated background and response files were downloaded. We used the *Swift*-XRT online pipeline to create the lightcurve. The observations were conducted in photon counting (PC) mode.

To determine the X-ray flux of IGR J17591–2342 for epochs that were closest to the radio observation, we analysed the 0.5–10 keV spectra with XSPEC version 12.9 (Arnaud 1996). The data were best fit with an absorbed (Wilms et al. 2000) powerlaw model; `Tbabs×powerlaw` (C-stat/degrees of freedom = 269/240). The addition of a blackbody component did not improve the fits, or change the results. X-ray fluxes were determined using

the XSPEC convolution model `cf1ux`. Results are shown in Table 2. The equivalent hydrogen column density, N_{H} , was tied between epochs (and determined by jointly fitting all 17 *Swift* observations between MJDs 58342–58403, not just the three reported in Table 2). Leaving N_{H} free gave similar results for all but the August 18 observation, where the low count-rate and a degeneracy between the photon index Γ and N_{H} meant that we could not place good constraints on either parameter.

3. RESULTS AND DISCUSSION

3.1. *Radio and X-ray lightcurves*

Following its initial X-ray detection, IGR J17591–2342 first brightened for a few days reaching an initial X-ray peak around August 14 (MJD 58344), around the time of the first *Swift*-XRT observation. IGR J17591–2342 then faded steadily over the next ~ 5 days (Figure 1). The source then re-brightened, returning to a similar X-ray count rate as its initial X-ray peak, following which it remained detectable for the next ~ 80 days.

A few days after the initial X-ray peak, we conducted our first radio observation, detecting the source at 5.5 and 9 GHz. Over the next ~ 2 weeks, we observed IGR J17591–2342 a further two times. During these observations, the source showed a similar evolution as the X-rays, where the radio flux faded briefly, before re-brightening (Figure 1).

During our first ATCA observation the radio spectrum was consistent with flat (Figure 1 and Table 1). The spectrum steepened slightly at the time of our second radio observation, although low signal to noise and frequency coverage meant the constraints on the spectrum were not strong. For our final radio observation, we observed the radio spectrum become significantly inverted. These observations of IGR J17591–2342 imply partially self-absorbed synchrotron emission from a steady compact jet (e.g. Fender 2001).

Table 2. Best-fitting spectral parameters for the 0.5–10 keV *Swift*-XRT observations that were closest in time to the ATCA radio observations. The data were fit with `Tbabs×powerLaw` within `XSPEC`. MJDs correspond to the mid-point of the X-ray observation (errors represent the observation duration). The column density along the line of sight, N_{H} , was tied between epochs to give $N_{\text{H}}=(4.4\pm 0.3)\times 10^{22}\text{ cm}^{-2}$. Γ is the photon index of the powerlaw component. Fluxes were calculated using `cflux`. Errors are $1\text{-}\sigma$.

Date	MJD	Obs ID	Γ	Absorbed	Unabsorbed
				1–10 keV Flux ($\times 10^{-10}$) $\text{erg s}^{-1}\text{ cm}^{-2}$	1–10 keV Flux ($\times 10^{-10}$) $\text{erg s}^{-1}\text{ cm}^{-2}$
2018 Aug 14	58344.688 \pm 0.002	00010804004	1.55 \pm 0.15	1.98 $^{+0.16}_{-0.15}$	2.96 $^{+0.17}_{-0.16}$
2018 Aug 18	58348.223 \pm 0.003	00010804004	2.1 \pm 0.3	0.79 $^{+0.11}_{-0.09}$	1.43 $^{+0.14}_{-0.13}$
2018 Aug 25	58355.559 \pm 0.033	00010804006	2.0 \pm 0.15	1.84 \pm 0.09	3.30 \pm 0.13

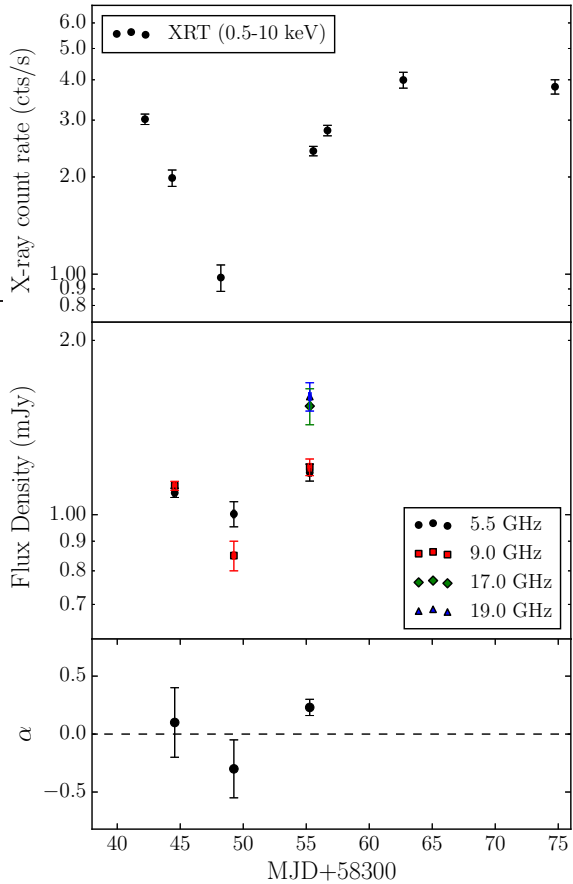


Figure 1. X-ray and radio lightcurves of IGR J17591–2342 during the early stages of its 2018 outburst. *Top panel:* 0.5–10 keV *Swift*-XRT observations. *Middle panel:* ATCA radio flux densities. *Bottom panel:* Radio spectral indices. Errors are $1\text{-}\sigma$.

3.2. Location on the radio/X-ray plane

To investigate the L_{R} and L_{X} of IGR J17591–2342, we place the 5 GHz radio and 1–10 keV X-ray luminosities on the radio/X-ray plane using several assumed distances (Figure 2). We convert our 5.5 GHz results to 5 GHz using the measured radio spectral index (including uncertainties). Unfortunately, our contemporaneous

observations sample only a very limited range of L_{R} and L_{X} (factors of only ~ 1.1 and ~ 2 , respectively). Therefore, while we are unable to determine the specific scaling between the L_{R} and L_{X} with this monitoring, the radio brightness introduces an interesting question: Is IGR J17591–2342 a radio-loud AMXP?

In terms of its radio and X-ray luminosities, for distances greater than ~ 3 kpc, IGR J17591–2342 would be brighter in the radio than the majority of other accreting NS systems (Figure 2). At a such distances, its $L_{\text{R}}/L_{\text{X}}$ ratio places IGR J17591–2342 in the region of parameter space occupied by BHXRBS. These results imply that IGR J17591–2342 was either considerably radio-loud during the early stages of its 2018 outburst, or it is closer than 3 kpc.

Comparing the observed radio emission from IGR J17591–2342 to the sample of AMXPs with reported radio detections (Figure 2, magenta squares), we see that IGR J17591–2342 appears to be more radio bright than all other NS systems for distances greater than ~ 5 kpc, where this reduces to ~ 3 kpc without the inclusion of the AMXP IGR J17379–3747 (although $L_{\text{X}} < 10^{36}\text{ erg s}^{-1}$ is not well explored). The recent radio detection of IGR J17379–3747 (van den Eijnden et al. 2018a) indicate this source as another potentially radio bright AMXP (Figure 2, magenta star), where an 8 kpc distance upper-limit was estimated from type I X-ray bursts, assuming that the peak flux of X-ray bursts reached the empirical NS Eddington limit.

3.3. Absorption along the line of sight

The soft X-ray emission observed from IGR J17591–2342 is highly absorbed. Using ISM abundances from Wilms et al. (2000), we find a best fit from *Swift*-XRT data of $N_{\text{H}}=(4.4\pm 0.3)\times 10^{22}\text{ cm}^{-2}$. This is consistent with results presented by Sanna et al. (2018), where the N_{H} was determined to be $(3.6\pm 1.1)\times 10^{22}\text{ cm}^{-2}$ from *INTEGRAL*, *NuSTAR*, and *Swift*-XRT observations taken at similar times. Our result is marginally higher than that found using the *NICER* data taken on similar dates (August 15

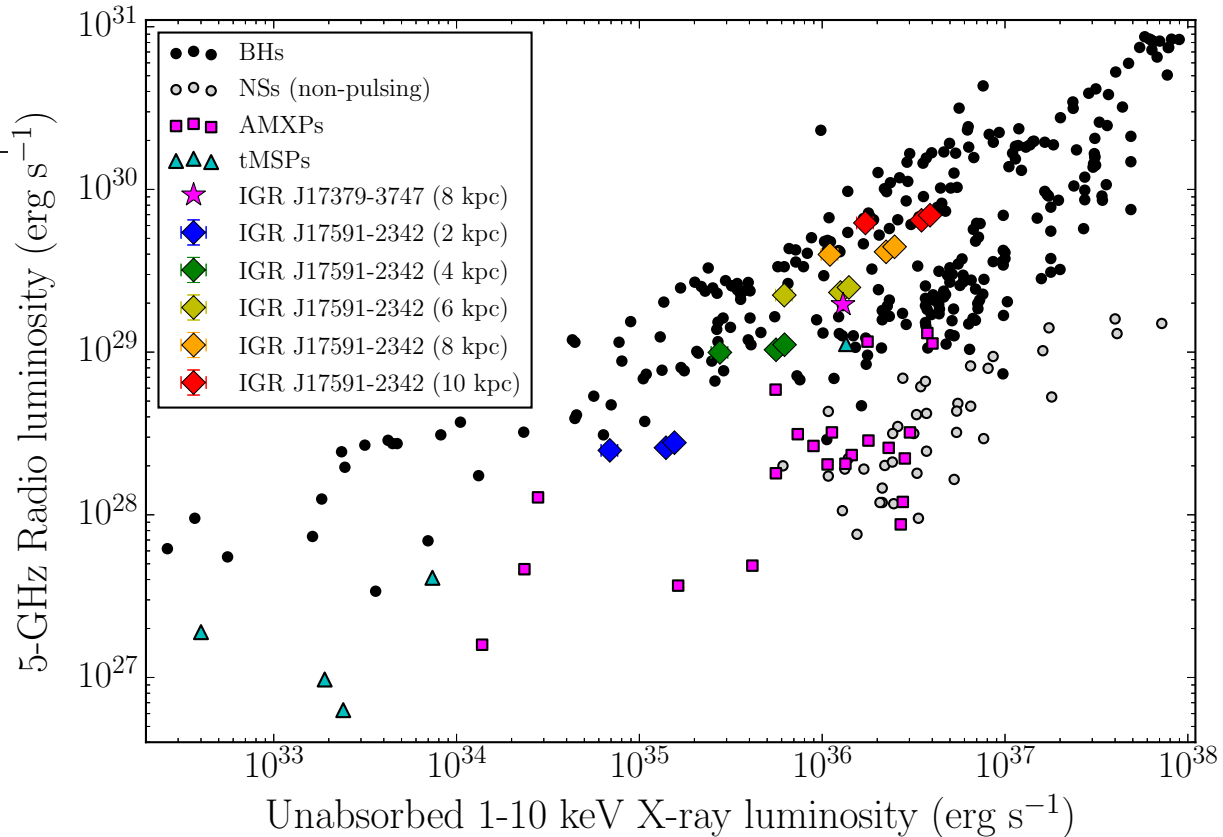


Figure 2. Radio/X-ray measurements of IGR J17591–2342 taken during the early stages of its 2018 outburst. This figure is adapted from [Bahramian et al. \(2018\)](#), and shows the radio/X-ray observations for different types of accreting stellar-mass compact objects (often multiple observations for the same source). IGR J17591–2342 is shown by the diamonds, where colours show different assumed distances (see Section 3.2). We also show other AMXPs (magenta squares), highlighting IGR J17379–3747 (magenta star) and tMSPs (cyan triangles). We see that at distances $\gtrsim 3$ kpc IGR J17591–2342 appeared more radio luminous than other NS systems at a similar X-ray luminosities. In fact, at such distances, IGR J17591–2342 lies in the region of parameter space usually occupied by black holes.

and August 18), which gave $(3.45^{+0.18}_{-0.15}) \times 10^{22} \text{ cm}^{-2}$ and $(3.59^{+0.05}_{-0.08}) \times 10^{22} \text{ cm}^{-2}$, respectively ([Sanna et al. 2018](#)), agreeing at the ~ 2 - σ level. Chandra observations taken on August 23 find $N_{\text{H}} = (4.9 \pm 0.2) \times 10^{22} \text{ cm}^{-2}$ ([Nowak et al. 2018](#)), consistent within the errors of our measured value.

IGR J17591–2342 lies in the direction of the Galactic center ([Ducci et al. 2018](#)), with an unknown distance to the source. However, our modelled N_{H} , which traces the interstellar gas along the line of sight, is ~ 3 – 4 times higher than the expected Galactic contribution of $N_{\text{HGal}} = 1.12$ – $1.44 \times 10^{22} \text{ cm}^{-2}$ ([Dickey & Lockman 1990](#); [Kalberla et al. 2005](#); [Willingale et al. 2013](#)). While such a discrepancy between the measured and expected N_{H} does not indicate the distance to the source, and the results may be dependent on the spectral model, it suggests that the source may be at a relatively large distance. To test the relationship with source distance, we compared the N_{HGal} ([Dickey & Lockman](#)

[1990](#); [Kalberla et al. 2005](#); [Willingale et al. 2013](#)) to the published¹ N_{H} for the 28 BH and NS XRBs with well estimated source distances² ([Gandhi et al. 2018](#); [Miller-Jones 2014](#), and references therein). We find that in all cases but two (GRS 1915+105 and V4641 Sgr) the measured N_{H} was either below or comparable to the expected Galactic line-of-sight absorption for these systems.

GRS 1915+105 and V4641 Sgr are both atypical and relatively distant BHXRBs (> 6 kpc), where the measured X-ray absorption exceeds the expected line of sight absorption by a factor of ~ 4 – 8 , due to anomalously high elemental abundances ([Orosz et al. 2001](#); [Lee et al. 2002](#)). For these systems, the overabundances

¹ To be consistent, when possible the N_{H} values taken from the literature were determined using a `Tbabs` spectral model.

² To test for differences between nearby and more distant objects.

are thought to be related to cold material in or near the local environment of the source (e.g. [Mirabel et al. 1996](#); [Martí et al. 2000](#); [Lee et al. 2002](#)). Other systems with unknown distances can also show higher than expected absorption, however, these are generally ascribed to their close proximity to the Galactic center (estimated from the high absorption; e.g. [Miller et al. 2006](#)), or are dipping sources, where disk material passes through the line of sight (e.g. [Parmar et al. 2002](#)).

There is some debate over the origin of the dominant X-ray absorber for XRBs, whether it be the ISM (even with highly ionized winds from the XRB; (e.g. [Miller et al. 2009](#)), or from gas intrinsic to the XRB (e.g. [Luo & Fang 2014](#)). However, from the high N_{H} (comparative to N_{HGal}), we favour the scenario in which IGR J17591–2342 is relatively distant (>5 kpc), likely close to the Galactic center (where the high absorption may arise from within the Galactic bulge; e.g. [Schultheis et al. 2014](#)). Such a distance would make IGR J17591–2342 a radio-loud NS system, with an L_{R} comparable to those observed from BHXRBS. Therefore, this result identifies the limitations of classifying XRBs from their $L_{\text{R}}/L_{\text{X}}$ ratio. However, it is important to note that the high N_{H} may arise from absorbing material intrinsic to the system, similar to what has been proposed for GRS 1915+105 and V4641 Sgr, allowing IGR J17591–2342 to be much more nearby. High-resolution X-ray spectroscopy is required to identify the overabundance of heavy elements ([Nowak et al. 2018](#)).

3.4. *Why is IGR J17591–2342 radio bright?*

While flaring from a transient jet or possibly a propeller mechanism could enhance the observed radio emission (e.g. [Tudor et al. 2017](#)), our observations suggest that the radio emission originated from a steady, compact jet.

For our first and third radio epochs, we observe a flat-to-inverted radio spectrum, inconsistent with emission from a transient jet (which would produce a steep radio spectrum). While the radio spectrum may have been steep during our second epoch, the flux remained stable over the three epochs arguing against significant flaring. Additionally, during the first epoch³ we did not detect intra-observation variability (down to 10 min timescales).

Furthermore, using system parameters determined by [Sanna et al. \(2018\)](#) and typical AMXP values, we expect a magnetic propeller regime to occur at an $L_{\text{X}} \lesssim 8 \times 10^{34} \text{ erg s}^{-1}$ ([Tsygankov et al. 2017](#)). Therefore, IGR J17591–2342 would need to be at distances

$\lesssim 1.5$ kpc for the observed radio emission to be propeller driven, which we find unlikely (Section 3.3).

There is thought to be some dependence between jet emission and spin for an accreting NS ([Parfrey et al. 2016](#)). IGR J17591–2342 is one of the more rapidly spinning AMXPs (527.4 Hz; [Sanna et al. 2018](#)). However, comparing its spin and radio luminosity with other AMXPs, there does not appear to be a clear relationship between these two properties. Therefore, while the NS spin may play some part in enhancing the jet emission in IGR J17591–2342, other characteristics, such as the magnetic field, NS mass, inclination, jet velocity, or launching mechanism, must play an important role in the observed jet emission of other systems (although the magnetic field of IGR J17591–2342 is typical of AMXP systems; [Sanna et al. 2018](#)).

4. CONCLUSIONS

Using quasi-simultaneous observations, we explore the radio and X-ray luminosities of IGR J17591–2342 during the early stages of its 2018 outburst. We find that the soft X-ray emission from the source is highly absorbed. Therefore, either IGR J17591–2342 is relatively distant and exceptionally radio-loud, or the source is more nearby with a significant contribution to the absorption from material local to the source itself, similar to that observed in the BHXRBS GRS 1915+105 and V4641 Sgr. If IGR J17591–2342 is at >3 kpc, then our observations place it at radio luminosities more similar to those observed from BHXRBS than NS systems, which could mean that such radio-loud NSs would be a source of confusion when classifying XRBs according to their radio and X-ray luminosities.

We thank Jamie Stevens and the ATNF staff for their rapid scheduling of the ATCA observations, making this study possible. TDR thanks Tobias Beuchert, Alice Borghese, Guglielmo Mastroserio, Pikky Atri, Juan Hernández Santisteban and the Jetset group for helpful discussions. TDR acknowledges support from the Netherlands Organisation for Scientific Research (NWO) Veni Fellowship, grant number 639.041.646. ND and JvdE are supported by a NWO Vidi grant, awarded to ND. NVG acknowledges funding from NOVA. JWTH acknowledges funding from an NWO Vidi fellowship and from the European Research Council under the European Unions Seventh Framework Programme (FP/2007-2013)/ERC Starting Grant agreement no. 337062 (DRAGNET). JCAM-J is the recipient of an Australian Research Council Future Fellowship (FT140101082). The International Centre for Radio Astronomy Research is a joint venture between Curtin University and the

³ Which was the only epoch we could test (Section 2.1).

University of Western Australia, funded by the state government of Western Australia and the joint venture partners. The Australia Telescope Compact Array is part of the Australia Telescope National Facility which is funded by the Australian Government for operation as a National Facility managed by CSIRO. We acknowledge the use of public data from the Swift data archive. This

research has made use of NASA’s Astrophysics Data System (ADS).

Facilities: ATCA, *Swift*-XRT

Software: CASA, XSPEC

REFERENCES

- Alpar, M. A., Cheng, A. F., Ruderman, M. A., & Shaham, J. 1982, *Nature*, 300, 728
- Archibald, A. M., et al. 2009, *Science*, 324, 1411
- Arnaud, K. A. 1996, in *Astronomical Society of the Pacific Conference Series*, Vol. 101, *Astronomical Data Analysis Software and Systems V*, ed. G. H. Jacoby & J. Barnes, 17
- Bahramian, A., et al. 2018, *Radio/X-ray correlation database for X-ray binaries*
- Blandford, R. D., & Königl, A. 1979, *ApJ*, 232, 34
- Bozzo, E., Ducci, L., Ferrigno, C., Savchenko, V., Kuulkers, E., Grinberg, V., Paizis, A., & Sidoli, L. 2018, *The Astronomer’s Telegram*, 11942
- Corbel, S., Coriat, M., Brocksopp, C., Tzioumis, A. K., Fender, R. P., Tomsick, J. A., Buxton, M. M., & Bailyn, C. D. 2013, *MNRAS*, 428, 2500
- Dickey, J. M., & Lockman, F. J. 1990, *ARA&A*, 28, 215
- Ducci, L., Kuulkers, E., Grinberg, V., Paizis, A., Sidoli, L., Bozzo, E., Ferrigno, C., & Savchenko, V. 2018, *The Astronomer’s Telegram*, 11941
- Evans, P. A., et al. 2009, *MNRAS*, 397, 1177
- Fender, R. P. 2001, *MNRAS*, 322, 31
- Fender, R. P., & Kuulkers, E. 2001, *MNRAS*, 324, 923
- Ferrigno, C., et al. 2018, *The Astronomer’s Telegram*, 11958
- Gallo, E., Degenaar, N., & van den Eijnden, J. 2018, *MNRAS*, 478, L132
- Gallo, E., Miller, B. P., & Fender, R. 2012, *MNRAS*, 423, 590
- Gallo, E., et al. 2014, *MNRAS*, 445, 290
- Gandhi, P., Rao, A., Johnson, M. A. C., Paice, J. A., & Maccarone, T. J. 2018, *ArXiv e-prints*
- in ’t Zand, J. J. M., Heise, J., Muller, J. M., Bazzano, A., Cocchi, M., Natalucci, L., & Ubertini, P. 1998, *A&A*, 331, L25
- Kalberla, P. M. W., Burton, W. B., Hartmann, D., Arnal, E. M., Bajaja, E., Morras, R., & Pöppel, W. G. L. 2005, *A&A*, 440, 775
- Krimm, H. A., et al. 2018, *The Astronomer’s Telegram*, 11981
- Lee, J. C., Reynolds, C. S., Remillard, R., Schulz, N. S., Blackman, E. G., & Fabian, A. C. 2002, *ApJ*, 567, 1102
- Luo, Y., & Fang, T. 2014, *ApJ*, 780, 170
- Maccarone, T. J. 2008, in *Astronomical Society of the Pacific Conference Series*, Vol. 401, *RS Ophiuchi (2006) and the Recurrent Nova Phenomenon*, ed. A. Evans, M. F. Bode, T. J. O’Brien, & M. J. Darnley, 191
- Martí, J., Mirabel, I. F., Chaty, S., & Rodríguez, L. F. 2000, *A&A*, 356, 943
- Martí-Vidal, I., Vlemmings, W. H. T., Muller, S., & Casey, S. 2014, *A&A*, 563, A136
- McMullin, J. P., Waters, B., Schiebel, D., Young, W., & Golap, K. 2007, in *Astronomical Society of the Pacific Conference Series*, Vol. 376, *Astronomical Data Analysis Software and Systems XVI*, ed. R. A. Shaw, F. Hill, & D. J. Bell, 127
- Migliari, S., & Fender, R. P. 2006, *MNRAS*, 366, 79
- Miller, J. M., Cackett, E. M., & Reis, R. C. 2009, *ApJL*, 707, L77
- Miller, J. M., et al. 2006, *ApJ*, 646, 394
- Miller-Jones, J. C. A. 2014, *PASA*, 31, e016
- Mirabel, I. F., Rodríguez, L. F., Chaty, S., Sauvage, M., Gerard, E., Duc, P.-A., Castro-Tirado, A., & Callanan, P. 1996, *ApJL*, 472, L111
- Nowak, M., Paizis, A., Chenevez, J., Chaty, S., Wilms, J., & Rodríguez, J. 2018, *The Astronomer’s Telegram*, 11988
- Orosz, J. A., et al. 2001, *ApJ*, 555, 489
- Papitto, A., et al. 2013, *Nature*, 501, 517
- Parfrey, K., Spitkovsky, A., & Beloborodov, A. M. 2016, *ApJ*, 822, 33
- Parmar, A. N., Oosterbroek, T., Boirin, L., & Lumb, D. 2002, *A&A*, 386, 910
- Patruno, A., & Watts, A. L. 2012, *ArXiv e-prints*
- Radhakrishnan, V., & Srinivasan, G. 1982, *Current Science*, 51, 1096
- Russell, T., Degenaar, N., Wijnands, R., & van den Eijnden, J. 2018, *The Astronomer’s Telegram*, 11954
- Sanchez-Fernandez, C., Ferrigno, C., Chenevez, J., Kuulkers, E., Wijnands, R., Bazzano, A., Jonker, P., & Del Santo, M. 2018, *The Astronomer’s Telegram*, 12000

- Sanna, A., et al. 2018, *A&A*, 617, L8
- Schultheis, M., et al. 2014, *A&A*, 566, A120
- Stappers, B. W., et al. 2014, *ApJ*, 790, 39
- Tsygankov, S. S., Mushtukov, A. A., Suleimanov, V. F., Doroshenko, V., Abolmasov, P. K., Lutovinov, A. A., & Poutanen, J. 2017, *A&A*, 608, A17
- Tudor, V., et al. 2017, *MNRAS*, 470, 324
- van den Eijnden, J., et al. 2018a, *The Astronomer's Telegram*, 11487
- van den Eijnden, J., Degenaar, N., Russell, T. D., Wijnands, R., Miller-Jones, J. C. A., Sivakoff, G. R., & Hernández Santisteban, J. V. 2018b, *ArXiv e-prints*
- Wijnands, R., & van der Klis, M. 1998, *Nature*, 394, 344
- Willingale, R., Starling, R. L. C., Beardmore, A. P., Tanvir, N. R., & O'Brien, P. T. 2013, *MNRAS*, 431, 394
- Wilms, J., Allen, A., & McCray, R. 2000, *ApJ*, 542, 914